

The Bipolar Field-Effect Transistor: VIII. Longitudinal Gradient of Longitudinal Electric Field (Two-MOS-Gates on Pure-Base)*

Jie Binbin(揭斌斌)^{1,2,†} and Sah Chih Tang(薩支唐)^{1,2,3,†}

(1 Department of Physics, Xiamen University, Xiamen 361005, China)

(2 CTSAH Associates, Gainesville, Florida 32605, USA)

(3 Chinese Academy of Sciences, Beijing 100864, China)

Abstract: This paper evaluates the electric current terms from the longitudinal gradient of the longitudinal electric field in Bipolar Field-Effect-Transistors (BiFETs) with a pure base and two MOS gates operating in the unipolar (electron) current mode. These nMOS-BiFETs, known as nMOS-FinFETs, usually have electrically short channels compared with their intrinsic Debye length of about 25 μm at room temperatures. These longitudinal electric current terms are important short-channel current components, which have been neglected in the computation of the long-channel electrical characteristics. This paper shows that the long-channel electrical characteristics are substantially modified by the longitudinal electrical current terms when the physical channel length is less than 100 nm.

Key words: bipolar field-effect transistor; pure base; intrinsic Debye length; long-channel characteristics; short-channel correction

DOI: 10.1088/1674-4926/31/7/071001

PACC: 7340Q

EEACC: 2560S; 2560B

1. Introduction

The theory of Bipolar Field-Effect Transistor (BiFET) has been reported by us in this series of the invited papers in the Journal of Semiconductors. The physical realization of the BiFETs was first described by us in the 2009 February issue^[1]. The BiFET CMOS voltage inverter circuit was realized by us with a single physical transistor, and its voltage–voltage and current–voltage characteristics were computed and presented in the 2008 November issue^[2]. The long-channel electrical characteristics of the nMOS-BiFET with pure base, under the unipolar (electron) current operation mode, were computed and reported in the 2009 March issue^[3].

As discussed in our 2007 November article^[4], the MOS-BiFETs with pure base are always electrically short compared with the physical lengths of the transistors, because there are so few electrons and holes to screen the charges (fixed ions, electrode charges, or mobile electron and hole charges), resulting in a linear carrier-screening distance (the Debye length) of about 25 μm . Recently, the physical length of the silicon transistors has decreased into the nanometer range. Thus, it is practically very important to know how good the computed long-channel electrical characteristics are for the today's transistors. This paper will answer this question by evaluating the current components from the longitudinal gradient of the longitudinal electric field. These terms are referred as the short-channel corrections in this paper.

2. The Drift–Diffusion and Electrochemical Current Theories

Two equivalent representations of the theoretical DC

current–voltage characteristics of the Bipolar Field-Effect Transistors have been described by us in this series of the invited papers. In the bipolar electrochemical current theory^[5], the electron and hole currents are calculated by integrations of the gradient of the electron and hole electrochemical potentials. In the bipolar drift and diffusion current theory^[6], the electron and hole currents are grouped into many drift and diffusion current components. Both representations are used to compute the characteristics in this paper. The device structure of an nMOS-BiFET was given in Fig. 1 of Ref. [3]. The corresponding boundary conditions are given by Eqs. (1) and (2) of Ref. [3]. The rigorous derivation of the equations for both representations is not repeated here, but the necessary assumptions are summarized here: (1) The three-dimensional electron and hole volume concentrations, $N(x, y, z)$ and $P(x, y, z)$, are exponential expressions of their thermal-voltage-normalized electrochemical potentials $U_N(x, y, z)$ and $U_P(x, y, z)$ and the electrostatic potential $U(x, y, z)$. This exponential transform is known as the Boltzmann representation^[7]. (2) Near thermal equilibrium with no hot carrier effects, the electron and hole mobilities and diffusivities closely follows the equilibrium Einstein Relationship $D_n/\mu_n = k_B T/q = D_p/\mu_p$ ^[7]. (3) The two-dimensional transistor problem is decomposed into two coupled one-dimensional problems by assuming the x -independence of the electron and hole electrochemical potentials, first introduced by Sah in 1965 and used by Pao and Sah^[8].

The transverse equations or X equations consist of two equations: the Gate-Voltage-Surface-Potential equation, Eq. (59) of Ref. [5], and the Base-Thickness-Surface-Potential equation, Eq. (60) of Ref. [5]. By neglecting the terms in the oxide and in the silicon surface layer arisen from the

* This investigation has been supported by the CTSAH Associates (CTSA), founded by the late Linda Su-Nan Chang Sah.

† Corresponding author. Email: bb_jie@msn.com and tom_sah@msn.com

Received 12 May 2010, revised manuscript received 20 May 2010

longitudinal gradient of the longitudinal electric field, given by Eq. (56) of Ref. [5], the two X equations are reduced to the Voltage equation (3) and the Thickness equation (4) of Ref. [3]. For easy of reference, these two simplified X equations for nMOS-BiFETs with the pure base are copied here:

The Voltage Equation: (X -equation)

$$U_{GB} - U_S = \text{sign}(U_S - U_0) \times (C_{Di}/C_O) \times [\exp(U_S - U_N) - \exp(U_0 - U_N) + \exp(U_P - U_S) - \exp(U_P - U_0)]^{1/2}. \quad (1)$$

The Thickness Equation: (X -equation)

$$X_B = 2 \int \text{sign}(U - U_0) \partial_X U \times [\exp(U - U_N) - \exp(U_0 - U_N) + \exp(U_P - U) - \exp(U_P - U_0)]^{-1/2}. \quad (2)$$

With the neglect of the longitudinal gradient of the longitudinal electric field and with the constancy of the electron mobility and diffusivity, the electron current in the electrochemical-potential representation reads:

$$\begin{aligned} I_N = 2qD_n n_i L_{Di}(W/L) \times \int \exp(-U_N) \partial U_N & \quad U_N = U_{SB} \text{ to } U_{DB} \\ \times \int \text{sign}(U - U_0) \exp(+U) \partial_x U & \quad U = U_0 \text{ to } U_S \\ \times [\exp(U - U_N) - \exp(U_0 - U_N) + \exp(U_P - U) - \exp(U_P - U_0)]^{-1/2}, & \quad (3) \end{aligned}$$

and in the drift–diffusion representation:

$$\begin{aligned} I_N = +kT\mu_n n_i L_{Di}(W/L) \times \left\{ + \int (-P/n_i) (\partial U / \partial Y) \partial X \right. & \quad \text{bulk charge drift term} \\ & + (\partial / \partial Y) [(C_O / C_{Di}) \times (2U_{GB} \times U_S - U_S^2)] \quad \text{carrier space-charge drift term} \\ & \left. + (\partial / \partial Y) \int (\partial U / \partial X)^2 \partial X \right\} \quad \text{transverse electric-field drift term} \\ + qD_n n_i L_{Di}(W/L) \times \left\{ - (\partial / \partial Y) \int (-P/n_i) \partial X \right. & \quad \text{bulk charge diffusion term} \\ & \left. + (\partial / \partial Y) [(C_O / C_{Di}) \times 2U_S] \right\}. \quad \text{carrier space-charge diffusion term} \quad (4) \end{aligned}$$

The “bulk-charge” drift and diffusion terms in the above equation can be neglected because of the pure base. It is important to note that “bulk-charge” consists of the ionized impurity charge ($P_{IM} = 0$) and the holes in the volume (P). The bulk-charge current term from the impurity charge is exactly zero due to the pure base. The bulk-charge term from the holes in the volume is negligibly small, which is proven by numerical comparison between the long-channel electron current in the electrochemical potential representation, Eq. (3), and the following long-channel electron current in the drift–diffusion representation without the bulk-charge terms in Eq. (4):

$$\begin{aligned} I_N = +kT\mu_n n_i L_{Di}(W/L) \times \left\{ + (\partial / \partial Y) [(C_O / C_{Di}) \times (2U_{GB} \times U_S - U_S^2)] \right. & \quad \text{carrier space-charge drift term} \\ & \left. + (\partial / \partial Y) \int (\partial U / \partial X)^2 \partial X \right\} \quad \text{transverse electric-field drift term} \\ + qD_n n_i L_{Di}(W/L) \times \left\{ + (\partial / \partial Y) [(C_O / C_{Di}) \times 2U_S] \right\}. & \quad \text{carrier space-charge diffusion term} \quad (5) \end{aligned}$$

Including the longitudinal gradient of the longitudinal electric field, derived from Eq. (15) of Ref. [6] as a verification of Sah’s 1995 theory^[9], two short-channel current components with the pre-factor $(L_{Di}/L)^2$ must be added to the long-channel electron current given by Eq. (5):

$$\begin{aligned}
 I_N = & + kT\mu_n n_i L_{Di}(W/L) \times \left\{ + (\partial/\partial Y)[(C_O/C_{Di}) \times (2U_{GB} \times U_S - U_S^2)] \right. && \text{carrier space-charge drift term} \\
 & + (\partial/\partial Y) \int (\partial U/\partial X)^2 \partial X && \text{transverse electric-field drift term} \\
 & \left. - (L_{Di}/L)^2 \partial/\partial Y \int (\partial U/\partial Y)^2 \partial X \right\} && \text{short-channel drift correction} \\
 & + qD_n n_i L_{Di}(W/L) \times \left\{ + (\partial/\partial Y)[(C_O/C_{Di}) \times 2U_S] \right. && \text{carrier space-charge diffusion term} \\
 & \left. + 2(L_{Di}/L)^2 (\partial/\partial Y) \int (\partial^2 U/\partial Y^2) \partial X \right\}. && \text{short-channel diffusion correction} \quad (6)
 \end{aligned}$$

The detailed explanation on how to numerically estimate these two short-channel current components was given in Ref. [10]. The equations given in Ref. [10] are listed in this paper for easy of reference. The electron electrochemical potential, U_{N1} , at any position $Y_1 = y_1/L$ along the longitudinal or y direction can be numerically solved by the Newton–Raphson method from the following implicit integration equation:

$$\begin{aligned}
 Y_1 = & 2qD_n n_i L_{Di}(W/L) \div I_N \times \int \exp(-U_N) \partial U_N && U_N = U_{SB} \text{ to } U_{N1} \\
 & \times \int \text{sign}(U - U_0) \exp(+U) \partial_x U && U = U_0 \text{ to } U_S \\
 & \times [\exp(U - U_N) - \exp(U_0 - U_N) + \exp(U_P - U) - \exp(U_P - U_0)]^{-1/2}. && (7)
 \end{aligned}$$

From this equation, Eq. (7), and the two X equations, Eqs. (1) and (2), the first derivative and second derivative of the potentials U_S and U_0 with respect to the Y position can be computed numerically. The two integrations in the two short-channel current components are estimated by:

$$\int (\partial U/\partial Y)^2 \partial X, X = 0 \text{ to } X_B, \approx [(\partial U_S/\partial Y)^2 + (\partial U_0/\partial Y)^2]/2 \times X_B, \quad (8)$$

$$\int (\partial^2 U/\partial Y^2) \partial X, X = 0 \text{ to } X_B, \approx [\partial^2 U_S/\partial Y^2 + \partial^2 U_0/\partial Y^2]/2 \times X_B. \quad (9)$$

Since the hole current in the nMOS-BiFET is zero, the drain terminal current I_D is the electron current I_N . From Eq. (6), the drain current consists of two parts: the long channel current I_{DL} and the short-channel correction I_{DS} . With the assumption that the short-channel correction does not change the drain current I_D significantly as the initial approximation, integrating Eq. (6) from $Y = 0$ to $Y = Y_1$, the following relations are obtained:

$$\begin{aligned}
 Y_1 \times I_{DL} = & + 2kT\mu_n n_i L_{Di}(W/L) \times \left\{ (C_O/C_{Di}) \times [(2U_{GS} \times U_S - U_S^2)|_{Y=Y_1} - (2U_{GS} \times U_S - U_S^2)|_{Y=0}] \right. \\
 & + (-1) \int [\exp(U - U_N) - \exp(U_0 - U_N) + \exp(U_P - U) - \exp(U_P - U_0)]^{1/2} \partial U|_{Y=Y_1} \\
 & \left. - (-1) \int [\exp(U - U_N) - \exp(U_0 - U_N) + \exp(U_P - U) - \exp(U_P - U_0)]^{1/2} \partial U|_{Y=0} \right\} \\
 & + qD_n n_i L_{Di}(W/L) \times \left\{ (C_O/C_{Di}) \times [2U_S|_{Y=Y_1} - 2U_S|_{Y=0}] \right\}, \quad (10)
 \end{aligned}$$

$$\begin{aligned}
 Y_1 \times I_{DS} = & + 2kT\mu_n n_i L_{Di}(W/L) \times \left\{ (L_{Di}/L)^2 \left[\int (\partial U/\partial Y)^2 \partial X|_{Y=Y_1} - \int (\partial U/\partial Y)^2 \partial X|_{Y=0} \right] \right\} \\
 & + 2qD_n n_i L_{Di}(W/L) \times \left\{ 2(L_{Di}/L)^2 \times \left[\int (\partial^2 U/\partial Y^2) \partial X|_{Y=Y_1} - \int (\partial^2 U/\partial Y^2) \partial X|_{Y=0} \right] \right\}. \quad (11)
 \end{aligned}$$

The drain terminal current, I_D , are then obtained by the sum of the above two equations. The corresponding drain conductances and transconductances are then computed by numerical derivatives or analytical derivative of the local (about five current points) least-squares-fit formula.

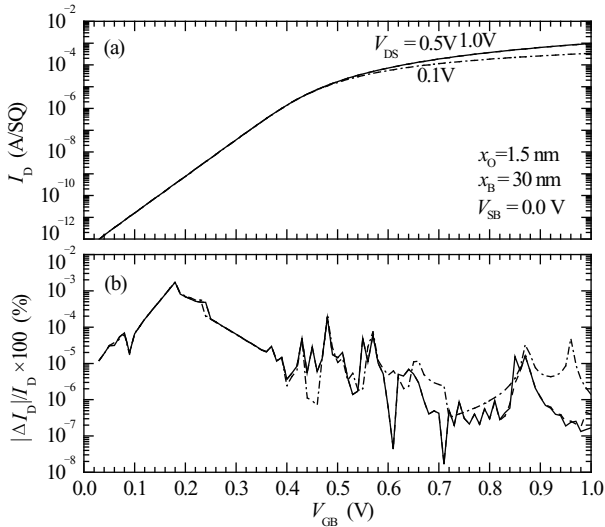


Fig. 1. Long-channel drain current versus gate voltage or transfer characteristics of an nMOS-BiFET with the oxide thickness $x_O = 1.5$ nm and the pure-base thickness $x_B = 30$ nm. (a) I_D - V_{GB} at $V_{DS} = 0.1, 0.5$ and 1.0 V and (b) the percentage difference between the long-channel drain currents computed in the electrochemical-potential representation and in the drift-diffusion representation. The difference in (b) is below the numeric noise level from the low-accuracy setting of Intel IMSL integration routine's relative accuracy of $10^{-2}\%$.

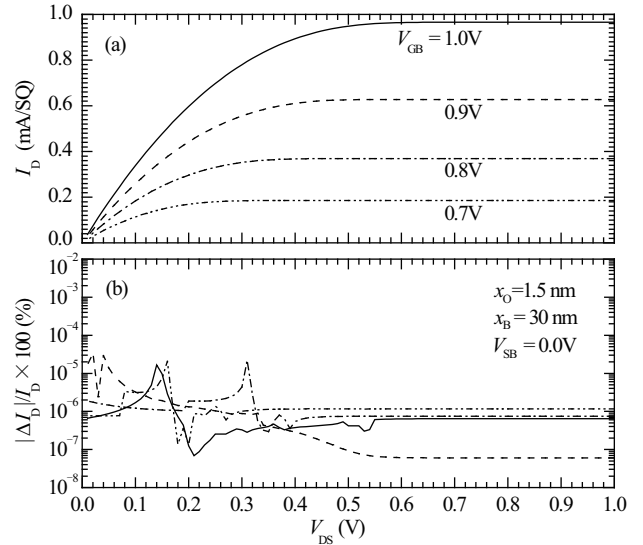


Fig. 2. Long-channel drain current versus drain voltage or output characteristics of an nMOS-BiFET with the oxide thickness $x_O = 1.5$ nm and the pure-base thickness $x_B = 30$ nm. (a) I_D - V_{DS} at $V_{GB} = 0.7, 0.8, 0.9$ and 1.0 V, and (b) the percentage difference between the long-channel drain currents computed in the electrochemical-potential representation and in the drift-diffusion representation. The difference in (b) is below the numeric noise level from the low-accuracy setting of Intel IMSL integration routine's relative accuracy of $10^{-2}\%$.

3. Computed Electrical Characteristics

3.1. Long-Channel Current-Voltage Characteristics

As described in Section 2, the negligible values of the bulk charge drift term and bulk charge diffusion term in Eq. (6) were expected from the pure base and proven by numerical comparison of the long-channel drain current in the electrochemical-potential representation and drift-diffusion representation. Figures 1 and 2 show this comparison for an nMOS-BiFET with the oxide thickness of $x_O = 1.5$ nm and the pure-base thickness of $x_B = 30$ nm. In the upper figures, (a), the long-channel drain currents, I_D , are plotted; in the lower figures, (b), the percentage difference between the long-channel drain currents in the electrochemical-potential representation and in the drift-diffusion representation, $|\Delta I_D|/I_D \times 100\%$, are plotted. Figure 1 shows the transfer characteristics with the constant V_{DS} at 0.1, 0.5 and 1.0 V. Figure 2 shows the output characteristics with the constant V_{GB} at 0.7, 0.8, 0.9 and 1.0 V. It is important to note that these computations were made using a Lenovo ThinkPad T60 computer with Microsoft Windows XP and the 64-bit Intel Visual Fortran (IVF) Compiler version 10.1 with IMSL Fortran Numerical Library Version 6.0. The IMSL integration routines have been intensively used by us to evaluate the integrations in the thickness equation and the electron current equation. The relative accuracy argument of the IMSL integration routines was set at a low accuracy of 10^{-4} , in order that the numerical iterations converge in a short time (several seconds). This low accuracy setting of the IMSL integration routines gave rise to the numeric noise level, in the percentage difference of the drain current, of the order of $10^{-4} \times 100\% = 10^{-2}\%$ or less. The lower figures in Figs. 1 and 2 show that the percentage difference between the long-channel drain currents from Eqs. (3) and (5) is well

below the numerical noise level $10^{-2}\%$. Thus, the bulk charge drift and diffusion terms are negligible, as anticipated for the pure base, $P_{IM} = 0$ and $N_{IM} = 0$ or $N_{DD} = 0$ and $P_{AA} = 0$.

3.2. Short-Channel Current-Voltage Characteristics

Figures 3 ($V_{DS} = 0.1$ V) and 4 ($V_{DS} = 0.5$ V) show the semilog plots of the long-channel current and short-channel correction of an nMOS-BiFET versus the gate terminal voltage V_{GB} at three cross-section planes $Y_1 = 0.50, 0.90$ and 0.99 . The channel length is $10 \mu\text{m}$, which is comparable to the intrinsic Debye length $L_{Di} \approx 25 \mu\text{m}$. The oxide thickness is 1.5 nm and the pure-base thickness is 30 nm. The source voltage is zero. The hole electrochemical potential is set at zero since we consider here zero hole currents with only one hole contact or two hole contacts tied together and grounded to serve as hole source. These two electron current components are evaluated at three positions $Y_1 = 0.50, 0.90$ and 0.99 . Consistent with current continuity, the long-channel currents are indeed nearly independent of the Y_1 position, because they dominate the total channel currents. As expected, the short-channel corrections (dashed lines in Figs. 3 and 4) increase when the Y_1 positions move towards the drain end. Because when the position Y_1 is closer to the drain end, the electron electrochemical potential increases exponentially with Y , leading to rapidly increasing longitudinal electric field, therefore, larger short-channel correction. But the short-channel corrections are so small that the total current is independent of the choice of Y as expected. Another feature in Figs. 3 and 4 is the subthreshold slope. For the long-channel currents, the slope is $\log_e 10 \times (k_B T/q) = 2.303 \times 25.85 \text{ mV} \approx 60 \text{ mV}$ per decade of current change from the E_X dependence^[9], which gives $\exp(qV_{GB}/k_B T)$ dependence. For the short channel cor-

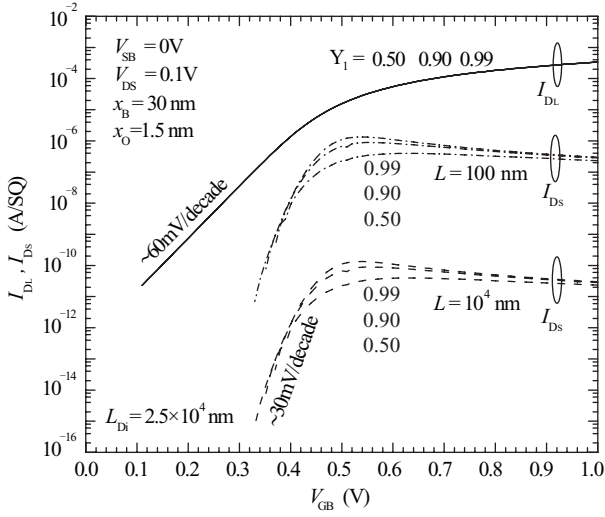


Fig. 3. Long-channel drain current I_{DL} and short-channel correction I_{DS} at positions $Y_1 = 0.50, 0.90$ and 0.99 are plotted versus the gate voltage V_{GB} with the drain voltage $V_{DS} = 0.1$ V. The channel length $L = 10 \mu\text{m}$ is comparable to the intrinsic Debye length $25 \mu\text{m}$.

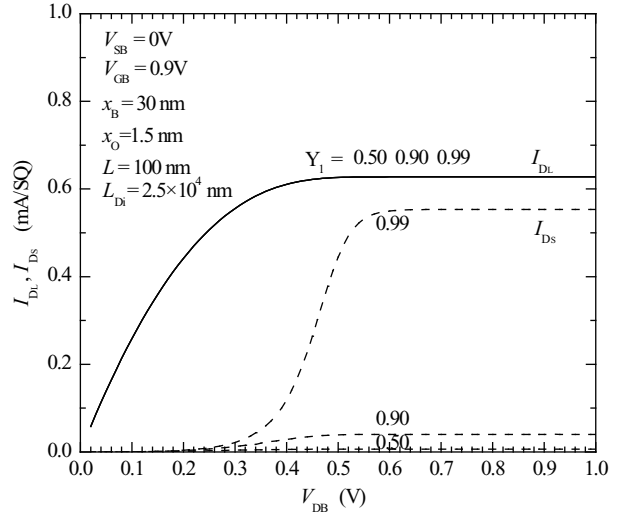


Fig. 5. Long-channel drain current I_{DL} and short-channel correction I_{DS} at positions $Y_1 = 0.50, 0.90$ and 0.99 are plotted versus the drain voltage V_{DB} with the drain voltage $V_{GB} = 0.9$ V. The channel length $L = 100$ nm.

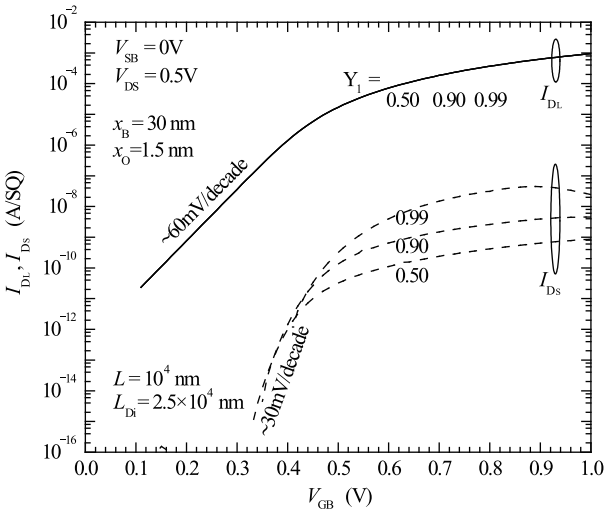


Fig. 4. Long-channel drain current I_{DL} and short-channel correction I_{DS} at positions $Y_1 = 0.50, 0.90$ and 0.99 are plotted versus the gate voltage V_{GB} with the drain voltage $V_{DS} = 0.5$ V. The channel length $L = 10 \mu\text{m}$ is comparable to the intrinsic Debye length $25 \mu\text{m}$.

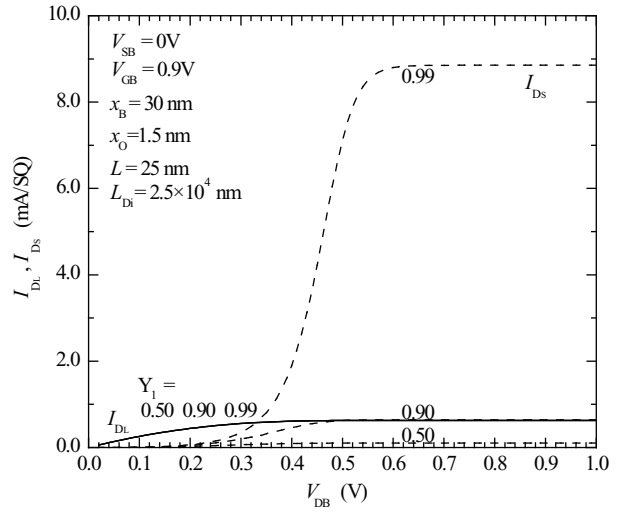


Fig. 6. Long-channel drain current I_{DL} and short-channel correction I_{DS} at positions $Y_1 = 0.50, 0.90$ and 0.99 are plotted versus the drain voltage V_{DB} with the drain voltage $V_{GB} = 0.9$ V. The channel length $L = 25$ nm.

rections, it is not more than 30 mV per decade from its E_x^2 or E_y^2 dependence (clearly seen in Sah's original formula in Ref. [9]), which gives $[\exp(qV_{GB}/k_B T)]^2$ dependence or a subthreshold voltage swing per decade of current change of $\log_e 10 \times (k_B T/q) \times (1/2) = 2.303 \times 25.85 \text{ mV} \times 0.5 \approx 30 \text{ mV}$.

In the strong "inversion" range, a reduction of the short channel correction current with the increasing gate voltage is observed in Fig. 3 for $V_{GB} > 0.5$ V at $V_{DS} = 0.1$ V and in Fig. 4 for $V_{GB} > 0.9$ V at $V_{DS} = 0.5$ V, or $V_{GB} - V_{DS} > 0.4$ V in both figures. The reason is that when the gate voltage is significantly larger than the drain voltage, the surface channel thickness is decreased from the source end all the way to the drain end with little V_{DS} effect, because the surface channel is very thin. This is equivalent to an increasing channel length at a constant chan-

nel thickness, thus, a reduction of the short-channel correction current. The factor of 0.4 V in $V_{GB} - V_{DS} > 0.4$ V comes from the needed ΔV_{GB} to overcome the barrier height difference between that at $n^{++}\text{S}/n_i\text{B}$ and $n_i\text{B}/n^{++}\text{D}$ junctions which controls of the two barrier heights by V_{GB} and $(V_{DB} - V_{SB}) = V_{DS}$.

The short-channel correction currents are at least four orders of magnitude smaller than the long-channel currents in Figs. 3 and 4, because the ratio of two current components $\exp(qV_{GB}/k_B T) = \exp(0.4/0.026) \approx 10^6$. Figures 5 and 6 show drain voltage dependence at two channel lengths, 100 nm and 25 nm, of the long-channel and short-channel correction currents at three Y_1 positions 0.50, 0.90 and 0.99 at a constant gate voltage of $V_{GB} = 0.9$ V. In Fig. 5, for the longer channel length $L = 100 \text{ nm} = L_{Di}/250$, the short-channel correction is much smaller than the long-channel currents until

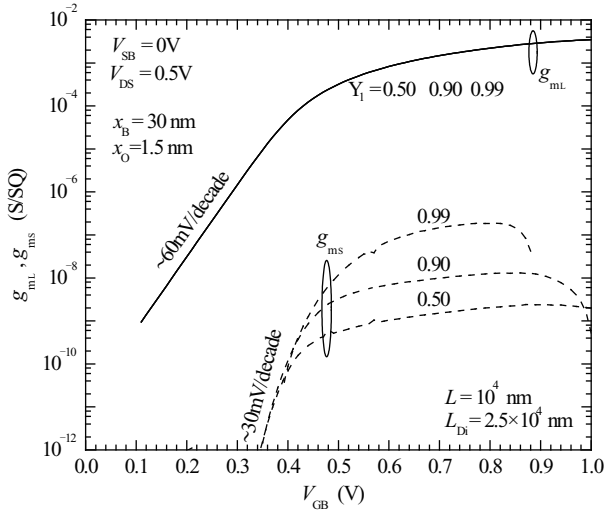


Fig. 7. Long-channel transconductance g_{mi} and short-channel correction g_{ms} at positions $Y_1 = 0.50, 0.90$ and 0.99 are plotted versus the gate voltage V_{GB} with the drain voltage $V_{DS} = 0.5$ V. The channel length $L = 10 \mu\text{m}$. Similar to Fig. 4.

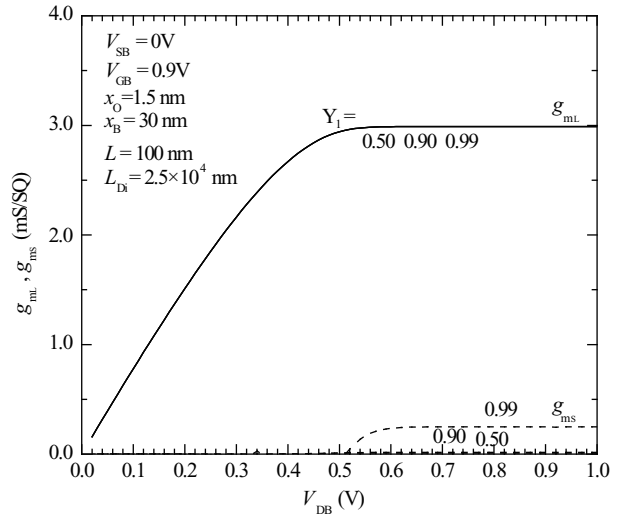


Fig. 9. Long-channel transconductance g_{mi} and short-channel correction g_{ms} at positions $Y_1 = 0.50, 0.90$ and 0.99 are plotted versus the drain voltage V_{DB} with the gate voltage $V_{GB} = 0.9$ V. The channel length $L = 100$ nm. Similar to Fig. 5.

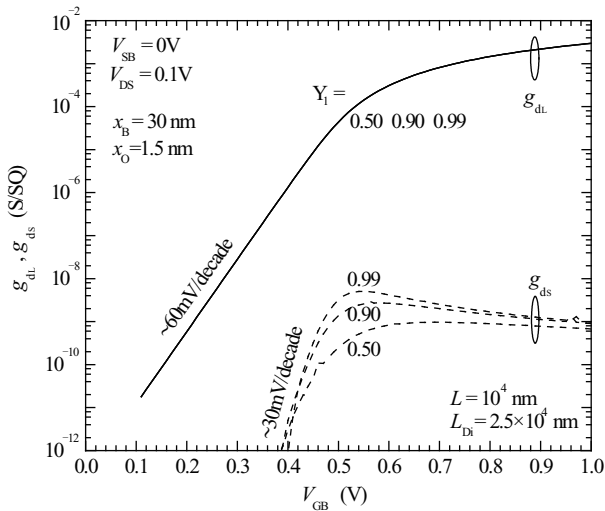


Fig. 8. Long-channel drain conductance g_{dl} and short-channel correction g_{ds} at positions $Y_1 = 0.50, 0.90$ and 0.99 are plotted versus the gate voltage V_{GB} with the drain voltage $V_{DS} = 0.1$ V. The channel length $L = 10 \mu\text{m}$. Similar to Fig. 3.

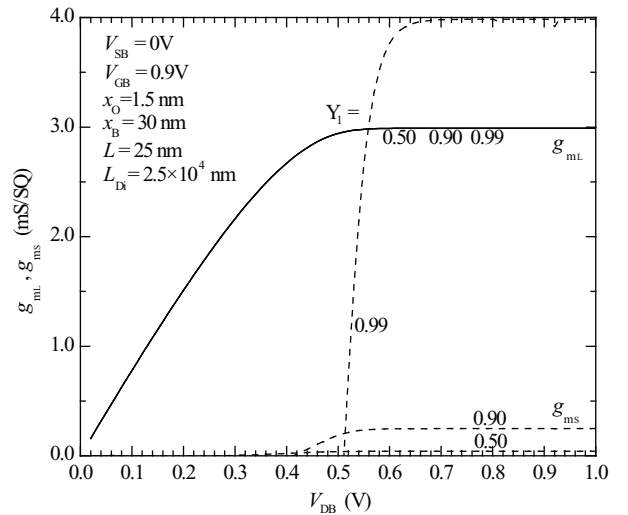


Fig. 10. Long-channel transconductance g_{mi} and short-channel correction g_{ms} at positions $Y_1 = 0.50, 0.90$ and 0.99 are plotted versus the drain voltage V_{DB} with the gate voltage $V_{GB} = 0.9$ V. The channel length $L = 25$ nm. Similar to Fig. 6.

$V_{DB} > \approx 0.5$ V or $V_{GB} - V_{DB} = 0.9$ V $- 0.5$ V = 0.4 V as explained before. In Fig. 6, for the shorter channel length of $L = 25$ nm = $L_{Di}/10^3$, the short-channel correction (using $Y_1 = 0.99$) is significantly (almost 20 times) larger than the long-channel current. So, the longitudinal electric field gradient cannot be neglected for current state-of-the-art transistors which channel length approaches 25 nm.

3.3. Drain Conductance and Transconductance Characteristics

To complete our analytical theory on the short channel effect due to carrier (Debye) screening, the slopes of $I-V$ curves, or the characteristics of drain conductance and transconductance are computed and shown in Figs. 7–12. The results are

self-explanatory and are further enhancements of the underlying device physics described for the $I-V$ curves in the preceding sections. A special feature, a peak in drain conductance near drain-current saturation, is shown in Figs. 11 ($L = 100$ nm) and 12 ($L = 25$ nm). This peak could be used as an experimental marker or fit parameter in device design characterization, such as the $V_{GB} - V_{DBpk} \approx 0.44$ V shift marked in Figs. 11 and 12.

4. Summary

This paper shows that the channel current from the quadratic term of the longitudinal electric field, or the longitudinal gradient of the longitudinal electric field, is very im-

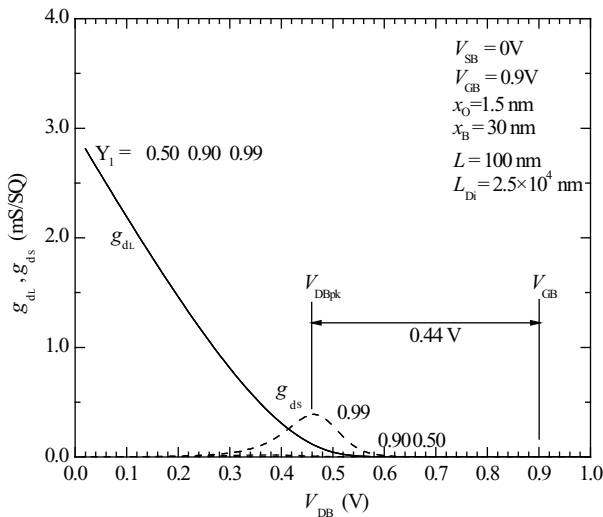


Fig. 11. Long-channel drain conductance g_{dl} and short-channel correction g_{ds} at positions $Y_1 = 0.50, 0.90$ and 0.99 are plotted versus the drain voltage V_{DB} with the gate voltage $V_{GB} = 0.9$ V. The channel length $L = 100$ nm.

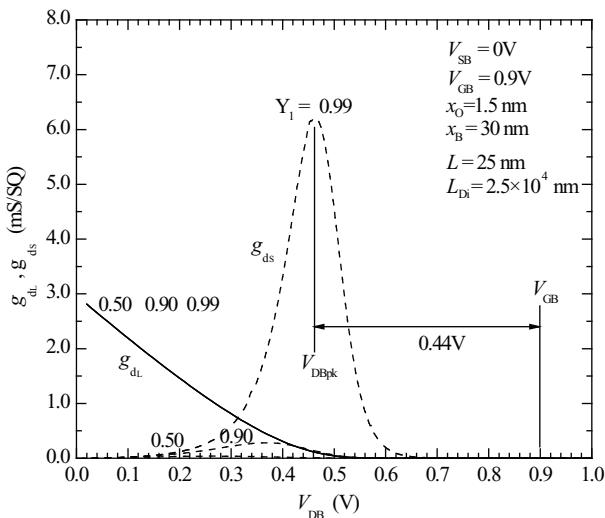


Fig. 12. Long-channel drain conductance g_{dl} and short-channel correction g_{ds} at positions $Y_1 = 0.50, 0.90$ and 0.99 are plotted versus the drain voltage V_{DB} with the gate voltage $V_{GB} = 0.9$ V. The channel length $L = 25$ nm.

portant in short channel MOSFETs as the channel length L decreases from 100 nm to 25 nm in pure and thin base, double MOS gates silicon field-effect transistors. The short-channel quadratic term is nearly twenty times higher than the long-channel term when L is about 25 nm. In the subthreshold range where diffusion current dominates, the short-channel term rises at 30 mV per decade of current which is twice faster than the long-channel term at the classical 60 mV per decade of current because of their different power dependence on the trans-

verse electric field, E_x and E_x^2 . At the threshold voltage when diffusion current dominates ($V_{GB} > \sim 400$ mV for our examples), compared with the long-channel current, the short-channel component is small $\sim 10^{-6}$ at 10^4 nm and is comparable ~ 1 at 10 nm. But at 100 nm in the strong inversion range when drift current dominates ($V_{GB} > 400$ mV), the short-channel component rises to become comparable to the long channel current.

This report is the first by the authors with affiliation to Xiamen University, China, for which we thank President Zhu Chongshi, School of Physics Dean Wu Chenxu, Department of Physics Chair Zhao Hong, and faculty and staff members. We thank the editor of the Journal of Semiconductors (formerly Chinese Journal of Semiconductors) for continued invitation to finish this series of articles on the bipolar theory of the field-effect transistors with the MOS and other gates.

References

- [1] Sah Chih-Tang and Jie Binbin, "The Bipolar Field-Effect Transistor: XIII. Physical Realizations of the Transistor and Circuits (One-Two-MOS-Gates on Thin-Thick Pure-Impure Base)," Journal of Semiconductors, 30(2), 021001-1-12, February 2009.
- [2] Jie Binbin and Sah Chih-Tang, "The Bipolar Field-Effect Transistor: VI. The CMOS Voltage Inverter Circuit (Two-MOS-Gates on Pure-Base)," Journal of Semiconductors, 29(11), 2079-2087, November 2008.
- [3] Jie Binbin and Sah Chih-Tang, "The Bipolar Field-Effect Transistor: VII. The Unipolar Current Mode for Analog-RF Operation (Two-MOS-Gates on Pure-Base)," Journal of Semiconductors, 30(3), 031001-1-8, March 2009.
- [4] Chih-Tang Sah and Bin B. Jie, "The Bipolar Field-Effect Transistor: I. Electrochemical Current Theory (Two-MOS-Gates on Pure-Base)," Chinese Journal of Semiconductors, 28(11), 1661-1673, November 2007.
- [5] Sah Chih-Tang and Jie Binbin, "The Theory of Field-Effect Transistors: XI. The Bipolar Electrochemical Currents (1-2-MOS-Gates on Thin-Thick Pure-Impure Base)," Chinese Journal of Semiconductors, 29(3), 397-409, March 2008.
- [6] Jie Binbin and Sah Chih-Tang, "The Theory of Field-Effect Transistors: XII. The Bipolar Drift and Diffusion Currents (1-2-MOS-Gates on Thin-Thick Pure-Impure Base)," Journal of Semiconductors, 29(7), 1227-1241, July 2008.
- [7] Chih-Tang Sah, Fundamentals of Solid State Electronics, 1001 pp, World Scientific Publishing Company, 2001.
- [8] Chih-Tang Sah and Bin B. Jie, "A History of MOS Transistor Compact Modeling," Keynote. Technical Proceedings Workshop on Compact Modeling (WCM), Abstract on pp. 1-2 and full text on pp. 349-390. Editors: Xing Zhou, Matthew Laudon and Bart Romanowicz. NSTI Nanotech2005, May 8-12, 2005. Online: <http://www.nsti.org/publ/Nanotech2005WCM/1429.pdf>.
- [9] Sah's 1995 derivation. Chih-Tang Sah, "Space Charge Theory of the MOS Transistor," version 1.1, 35 pages, December 12, 1996, Intel Research Grant Report, unpublished.
- [10] Bin B. Jie and Chih-Tang Sah, "Theory of Bipolar MOSFET (BiFET) with Electrically Short Channels," Technical Proceedings of NSTI-Nanotech 2010, vol. 3, Workshop on Compact Modeling, June 2010.